Current-induced spin polarization in the isotropic k-cubed Rashba model: Theoretical study of p-doped semiconductor heterostructures and perovskite-oxide interfaces

Ł. Karwacki,[1] A. Dyrdał,[2,3] J. Berakdar,[2] and J. Barnaś[1,3]

[1]*Institute of Molecular Physics, Polish Academy of Sciences, ul. M. Smoluchowskiego 17, 60-179 Poznań, Poland*

[2]*Institut für Physik, Martin-Luther Universität Halle-Wittenberg, D-06099 Halle, Germany*

[3]*Faculty of Physics, Adam Mickiewicz University, ul. Umultowska 85, 61-614 Poznań, Poland*

(Received 21 November 2017; revised manuscript received 24 March 2018; published 4 June 2018)

Using the Matsubara Green's function formalism, we calculate the temperature dependence of the nonequilibrium spin polarization induced by an external electric field in the presence of spin-orbit coupling. The model Hamiltonian includes an isotropic k-cubed form of the Rashba spin-orbit interaction. Such a Hamiltonian captures the electronic and the spin properties of a two-dimensional electron (hole) gas at the surfaces or interfaces of transition metal oxides or in p-doped semiconductor heterostructures. The induced spin polarization is calculated for the nonmagnetic as well as for a magnetic electron/hole gas. Relations of the spin polarization to the Berry curvature is also discussed.

DOI: 10.1103/PhysRevB.97.235302

I. INTRODUCTION

The efficient control of the electron spin is currently one of the key issues in spintronics. It is known that the spin-orbit interaction in low-dimensional systems is usually strongly enhanced and leads to new phases of matter that emerge at the interface [1–4], for instance, the chiral spin order, and to a spin polarization. Thus, pure electrical control of the spin degree of freedom seems to be a promising concept for future applications in electronics. Moreover, such control is also intriguing from a fundamental physics point of view. Indeed, the physics of low-dimensional heterostructures based on semiconductors, graphenelike materials, and oxides reveals a diversity of particular phenomena dictating electronic and spin transport [5–8].

One of the most prominent phenomena induced by the spin-orbit coupling is the spin Hall effect [9–11]. This effect has already become a standard tool for the generation and detection of spin currents [12–15]. Furthermore, spin Hall currents can generate a spin-torque and induce spin dynamics [16–19]. In this scenario, one needs no magnetic polarizer as required for spin-valve devices. The spin-orbit interaction may also lead to a spin polarization (a phenomenon known as the Edelstein effect or the inverse spin galvanic effect) when an external electric field is applied to the system [20–26]. In magnetic systems, this nonequilibrium spin polarization may interact via the exchange coupling with the local magnetization, giving rise to a spin torque.

In the context of the aforementioned issues, heterostructures of transition metal oxides are attracting much attention recently. Current experimental techniques allow for epitaxial growth of different high-quality perovskite oxides as to achieve artificially tailored heterostructures with relatively sharp interfaces [27–30]. The discovery of a two-dimensional (2D) electron gas at the interface of such structures like $LaAlO_3/SrTiO_3$ (LAO/STO) [28,31] offers a new route for materials and spintronics research, revealing a variety of interesting phenomena in these hetrostructures such as the colossal magnetoresistance, ferroelectricity, ferro-, and antiferromagnetism, through metal-insulator transitions and high-temperature superconductivity, and enhanced spin-orbit coupling [32–47].

Despite the fact that cubic perovskites, such as STO and STO-based structures, have been studied intensively, there are only a few experimental results that reveal properties of their conduction bands. Moreover, the physical picture of the spin-orbit interaction in 2D electron gas at the interfaces of perovskite oxides, being under intensive discussions in recent years, is still elusive.

First of all, the STO-based heterostructures reveal d-electron spin-orbit coupling [48–51]. The strongly anisotropic d-orbitals together with quantum confinement result in a complicated spin-orbit texture that is much richer than in the case of sp-electron gas in the conventional n-doped semiconductor heterostructures [52]. In the case of cubic perovskites, such as STO, the crystal field due to the octahedral coordination with neighboring oxygen atoms splits the degenerate atomic d-levels (originating mainly from Ti sites) into the threefold degenerate t_{2g} states and twofold degenerate e_g states [50,53,54]. The energy distance between these orbitals is about 2 eV. Therefore, low-energy effective models of electronic states in the vicinity of the Γ point of the Brillouin zone account only for the t_{2g} orbitals. The symmetry of the bottom of the conduction t_{2g} band (at the Γ point) is the same as the symmetry of the corresponding p-states in p-doped semiconductor heterostructures based on zincblende III–V semiconductors [54,55]. Accordingly, the spin-orbit coupling lifts the degeneracy at the Γ point further into heavy and light electron bands (with the total angular momentum $J = 3/2$) and a split-off band (with $J = 1/2$), similar to the heavy, light, and split-off hole bands in III–V semiconductors.

Recent experimental results based on weak localization and antilocalization effects in magnetoresistance indicate unambiguously the k-cubed character of the Rashba spin-orbit interaction in transition-metal oxides [55,56]. This is in

agreement with recent theoretical studies based on density functional theory (DFT) simulations and tight-binding modeling [54,60].

In this paper, we study in detail the current-induced spin polarization for an effective Hamiltonian describing 2D electron/hole gas with isotropic k-cubed Rashba spin-orbit interaction. The model Hamiltonian under consideration has the form of a 2×2 matrix, and has been derived by the perturbation procedure from the 8×8 Luttinger Hamiltonian for p-doped semiconductor quantum wells with structural inversion asymmetry [61]. Such a model was used to describe the experimentally observed 2D electron gas at the oxides interfaces [55]. Therefore, in this paper, we focus on the spin and the electronic transport properties of electron and hole gases, that in the first approximation can be described by the effective Hamiltonian with the isotropic k-cubed form of Rashba spin-orbit interaction. To describe the current-induced spin polarization we use the Matsubara Green's function formalism in the linear response regime. This allows us to analyze the nonequilibrium spin polarization also beyond the zero-temperature limit.

The paper is organized as follows. In Sec. II, we introduce the effective Hamiltonian and the necessary concepts for the analytical and numerical calculations. In Sec. III, we discuss the current-induced spin polarization and its temperature dependence in a nonmagnetic k-cubed Rashba gas. In Sec. IV, we present our results for the system in the presence of the exchange field. At first, we discuss some special cases, where the magnetization is oriented perpendicularly to the 2D gas plane and when it is oriented in the plane of 2D gas. At the end of this section, we also discuss the case of arbitrary oriented-exchange field. The final conclusions and outlook for future research are presented in Sec. V.

II. THEORETICAL OUTLINE

A. Model

We consider the effective Hamiltonian describing a 2D electron (hole) gas with an isotropic k-cubed Rashba spin-orbit interaction and subject to an exchange field. With some assumptions, such an effective Hamiltonian may be appropriate for the description of 2D electron gases (2DEG) at the interface between two oxide perovskites, for instance, LAO/STO [55], or for heavy-hole gas that appears in semiconductor heterostructures [52]. This Hamiltonian takes the following matrix form:

$$\hat{H} = \frac{\hbar^2 k^2}{2m}\sigma_0 + \mathrm{i}\lambda\left(k_-^3\sigma_+ - k_+^3\sigma_-\right) - \frac{1}{\hbar}\mathbf{H}\cdot\hat{\mathbf{S}}, \tag{1}$$

where the first term describes the kinetic energy with the effective mass defined by electron rest mass m_0 and Luttinger parameters $\gamma_{1,2}$ [61]:

$$m = m_0\left(\gamma_1 + \gamma_2 - \frac{256\gamma_2^2}{3\pi^2(3\gamma_1 + 10\gamma_2)}\right)^{-1}. \tag{2}$$

The second term describes the isotropic k-cubed Rashba spin-orbit interaction with $k_\pm = k_x \pm \mathrm{i}k_y$, $\sigma_\pm = (\sigma_x \pm \mathrm{i}\sigma_y)/2$ (here, σ_α with $\alpha = 0,x,y,z$ are the unit and Pauli matrices, respectively), and the Rashba coupling parameter defined as [61]

$$\lambda = \frac{512eFL_z^4\gamma_2^2}{9\pi^2(3\gamma_1 + 10\gamma_2)(\gamma_1 - 2\gamma_2)}, \tag{3}$$

where L_z and eF denote the width and the potential of the quantum well, respectively. The last term in Hamiltonian Eq. (1) describes the effect of exchange field due to the exchange interaction between electrons and local macroscopic magnetization. The exchange field $\mathbf{H}$ is oriented arbitrarily and its three components in the spherical coordinate system can be written as follows:

$$H_x = H_0\sin\theta\cos\xi, \tag{4}$$

$$H_y = H_0\sin\theta\sin\xi, \tag{5}$$

$$H_z = H_0\cos\theta, \tag{6}$$

where $H_0 = h_0[1 - (T/T_c)^{3/2}]$ with h_0 given in energy units and proportional to the exchange parameter and the saturation magnetization at $T = 0$, and T_c denoting the Curie temperature.

The Hamiltonian Eq. (1) has been obtained upon two canonical transformations, so the spin-operators, $\hat{S}_\alpha$, after the same unitary transformations have the form

$$\begin{aligned}\hat{S}_x &= -\hbar s_0 k_y\sigma_0 + \hbar s_1(k_-^2\sigma_+ + k_+^2\sigma_-)\\ &= -\hbar s_0 k_y\sigma_0 + \hbar s_1\left(k_x^2 - k_y^2\right)\sigma_x + 2\hbar s_1 k_x k_y\sigma_y,\end{aligned} \tag{7}$$

$$\begin{aligned}\hat{S}_y &= \hbar s_0 k_x\sigma_0 + \mathrm{i}\hbar s_1(k_-^2\sigma_+ - k_+^2\sigma_-)\\ &= \hbar s_0 k_x\sigma_0 + \hbar s_1\left(k_x^2 - k_y^2\right)\sigma_y - 2\hbar s_1 k_x k_y\sigma_x,\end{aligned} \tag{8}$$

$$\hat{S}_z = \frac{3}{2}\hbar\sigma_z, \tag{9}$$

where s_0 and s_1 are defined by the material parameters:

$$s_0 = \frac{512\gamma_2 L_z^4 eFm_0}{9\pi^6(3\gamma_1 + 10\gamma_2)(\gamma_1 - 2\gamma_2)\hbar^2}, \tag{10}$$

$$s_1 = L_z^2\left(\frac{3}{4\pi^2} - \frac{256\gamma_2^2}{3\pi^4(3\gamma_1 + 10\gamma_2)}\right), \tag{11}$$

(for details, see Ref. [61]). Thus, the effective mass as well as the Rashba parameter depend strongly on the material parameters. Variation of the Rashba parameter and the parameter s_0 with the quantum well width L_z and the electric field F (describing the asymmetric quantum well potential) are shown in Fig. 1. We present this dependence for Luttinger parameters $\gamma_{1,2}$ adequate for 2D hole gas (2DHG) in GaAs [52] [Figs. 1(a), 1(c), 1(e)] and for $\gamma_{1,2}$ obtained from fitting to experimental data and from DFT calculations for the LAO/STO interface [53,55,56] [Figs. 1(b), 1(d), 1(f)]. Thus, for fixed Luttinger parameters, the Rashba spin-orbit coupling increases with increasing electric field and width of the quantum well. A similar conclusion follows from the behavior of the s_0 parameter, which is shown in Figs. 1(e) and 1(f). Moreover, for chosen values of Luttinger parameters, the spin-orbit interaction is stronger in GaAs 2DHG than in LAO/STO 2DEG. We should also note that the transformations leading to Eq. (3) take into

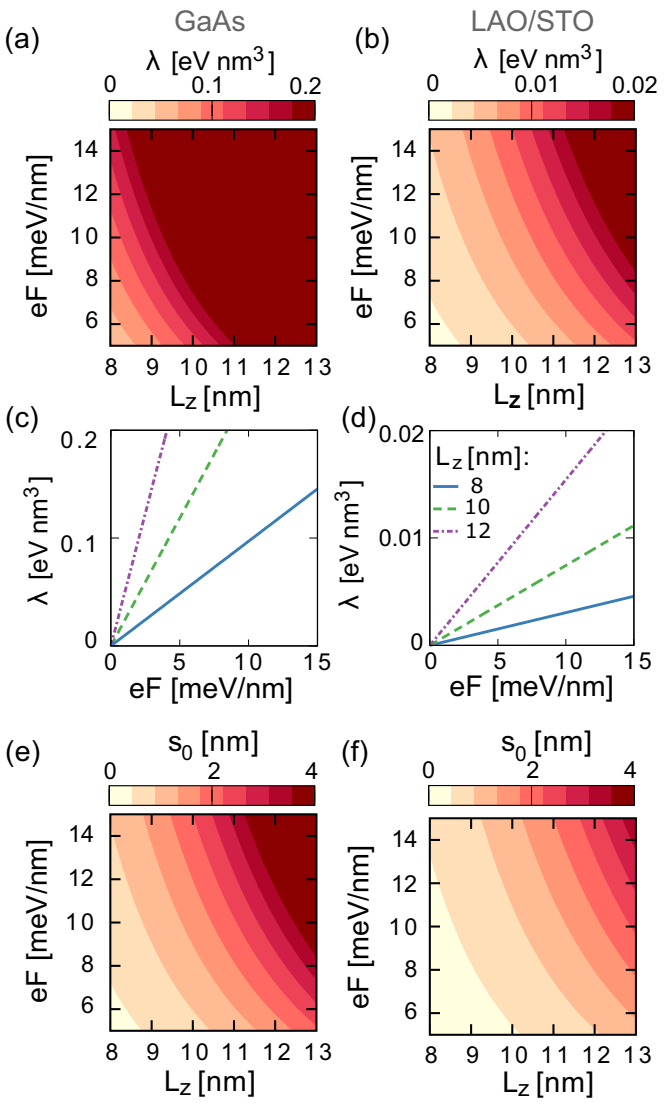

FIG. 1. Spin-orbit coupling strength λ as a function of the quantum well width L_z and the confining electric field F for GaAs (a) and for perovskite oxide (b); cross-sections of λ as functions of F for GaAs (c) and perovskite oxide (d); s_0 parameter as a function of quantum well width L_z and confining electric field F for GaAs (e) and perovskite oxide (f). Luttinger parameters: (GaAs) $\gamma_1 = 6.85$, $\gamma_2 = 2.145$ [52], (LAO/STO) $\gamma_1 = 1.9$, $\gamma_2 = 0.12$ [53,54] (see also comment in the text).

account only γ_1 and γ_2 parameters of the original Luttinger Hamiltonian. In the general case, however, an additional γ_3 parameter is present and may play a role when estimating the proper parameters of the system [52].

Our main focus is to work out the general behavior of the nonequilibrium spin polarization for a Hamiltonian with a specific functional form of the spin-orbit interaction. To be specific, we also discuss and compare experimental and numerical data as well as results obtained based on DFT and tight-binding calculations to estimate the Luttinger parameters suitable for a description of perovskite oxides. These parameters may be used further to check not only qualitatively but also quantitatively the magnitude of spin polarization or other spin and transport phenomena for specific perovskite interfaces. A summary of these parameters of concern are presented in Table. I.

B. Methods and general solutions

The nonequilibrium spin polarization created by the external electric field is calculated in the Matsubara Green function formalism. The general expression for the spin polarization that appears as a response to the external electric field can be written in the following form [62]:

$$S_\alpha(\mathrm{i}\omega_m) = \frac{1}{\beta}\sum_n \int \frac{d^2\mathbf{k}}{(2\pi)^2} \times \mathrm{Tr}\{\hat{S}_\alpha G_\mathbf{k}(\mathrm{i}\varepsilon_n + \mathrm{i}\omega_m)\hat{H}_\mathbf{A}(\mathrm{i}\omega_m)G_\mathbf{k}(\mathrm{i}\varepsilon_n)\}, \quad (12)$$

where $\beta = 1/k_BT$ (with T and k_B denoting the temperature and Boltzmann constant, respectively), $\varepsilon_n = (2n+1)\pi k_BT$ and $\omega_m = 2m\pi k_BT$ are the Matsubara energies, while $G_\mathbf{k}(\mathrm{i}\varepsilon_n)$ are the Matsubara Green functions (in the 2×2 matrix form). The perturbation term which describes the interaction of the electrons with an external electric field has the form

$$\hat{H}^E_\mathbf{A}(\mathrm{i}\omega_m) = -e\hat{v}_j A_j(\mathrm{i}\omega_m), \quad (13)$$

with the amplitude of the vector potential $A_j(\mathrm{i}\omega_m)$ determined by the amplitude $E_j(\mathrm{i}\omega_m)$ of electric field through the following relation: $A_j(\mathrm{i}\omega_m) = \frac{E_j(\mathrm{i}\omega_m)\hbar}{\mathrm{i}(\mathrm{i}\omega_m)}$. The summation over Matsubara frequencies in Eq. (12) can be performed using contour integration, and we find

$$S_\alpha(\mathrm{i}\omega_m) = -\frac{eE_j\hbar}{\mathrm{i}\omega_m}\mathrm{Tr}\int\frac{d^2\mathbf{k}}{(2\pi)^2} \times \int_\mathcal{C}\frac{dz}{2\pi}f(z)\hat{S}_\alpha G_\mathbf{k}(z+\mathrm{i}\omega_m)\hat{v}_j G_\mathbf{k}(z). \quad (14)$$

In the expression above, $f(z)$ is the meromorphic function of the form $[\exp(\beta z)+1]^{-1}$, which has simple poles at the odd integers n ($z = \mathrm{i}\varepsilon_n$), while $\mathcal{C}$ denotes an appropriate integration contour. After an analytical continuation [62] we find the general expression describing the nonequilibrium spin polarization in the following form [63]:

$$S_\alpha(\omega) = -\frac{e\hbar}{\omega}E_j\mathrm{Tr}\int\frac{d^2\mathbf{k}}{(2\pi)^2} \times \int\frac{d\varepsilon}{2\pi}f(\varepsilon)\hat{S}_\alpha\Big(G^R_\mathbf{k}(\varepsilon+\omega)\hat{v}_j\big[G^R_\mathbf{k}(\varepsilon)-G^A_\mathbf{k}(\varepsilon)\big] + \big[G^R_\mathbf{k}(\varepsilon)-G^A_\mathbf{k}(\varepsilon)\big]\hat{v}_j G^A_\mathbf{k}(\varepsilon-\omega)\Big) \quad (15)$$

where $f(\varepsilon)$ is the Fermi-Dirac distribution function and $\hat{v}_j$ is the j-th component of the velocity operator, $\hat{v}_j = (1/\hbar)\partial\hat{H}/\partial k_j$.

To make our further expressions more clear, let us rewrite the Hamiltonian Eq. (1) in the general form

$$\hat{H} = n_0\sigma_0 + \mathbf{n}\cdot\boldsymbol{\sigma}, \quad (16)$$

where $\mathbf{n} = (n_x, n_y, n_z)$ and $\boldsymbol{\sigma} = (\sigma_x, \sigma_y, \sigma_z)$. The coefficients n_i ($i = 0, x, y, z$) take then the following forms:

$$n_0 = \varepsilon_k + s_0(k_yH_x - k_xH_y), \quad (17)$$

$$n_x = -\lambda\big(k_y^3 - 3k_x^2k_y\big) - s_1H_x\big(k_x^2 - k_y^2\big) + 2H_ys_1k_xk_y, \quad (18)$$

TABLE I. Experimental, *ab initio*, and estimated Luttinger parameters for 2D electron gas at interfaces of perovskite oxides and for 2D hole gas at semiconductor interfaces (sharp parentheses denote parameters taken from other positions in the table).

	System	$n[10^{12}\mathrm{cm}^{-2}]$	m^*/m_0	λ [meV nm^3]	eF [meV/nm]	L_z [nm]	γ_1	γ_2
Heeringen *et al.* [53,54]	$SrTiO_3$		1.2	$\langle 2-1\rangle$	10	$\langle 10\rangle$	0.81–0.82	0.03-0.02
	$LaAlO_3/SrTiO_3$	7.2	0.5–1.5	$\langle 0.8\rangle$	1	10	1.9–0.63	0.12-0.04
Caviglia *et al.* [57]	$LaAlO_3/SrTiO_3$	10.5	∼1.45					
Nakamura *et al.* [55]	$SrTiO_3$	2–8	1.5	2-1	450	$\langle 10\rangle$	0.66	0.003-0.002
Liang *et al.* [56]	$LaAlO_3/SrTiO_3$	8–31	1.5	0.8-0.3				
	$LaVO_3/SrTiO_3$	14-30	1.5	0.5-0.4				
Hassan *et al.* [58]	$Ge/Si_{0.2}Ge_{0.8}$	∼0.6	∼0.06	79.7	$\langle 10-450\rangle$	12 ± 2	15.1-16.3	2.2-0.34
Moriya *et al.* [59]	$Ge/Si_{0.5}Ge_{0.5}$	1–1.5	∼0.08	20-14	$\langle 10-450\rangle$	$\langle 12\rangle$	11.8-12.4	0.85-0.13

$$n_y = -\lambda\left(k_x^3 - 3k_x k_y^2\right) - s_1 H_y\left(k_x^2 - k_y^2\right) - 2H_x s_1 k_x k_y, \quad (19)$$

$$n_z = -\frac{3}{2}H_z. \quad (20)$$

The retarded Green function may then be written as

$$G_{\mathbf{k}}^R(\varepsilon) = G_{\mathbf{k}0}^R\sigma_0 + G_{\mathbf{k}x}^R\sigma_x + G_{\mathbf{k}y}^R\sigma_y + G_{\mathbf{k}z}^R\sigma_z, \quad (21)$$

with the coefficients

$$G_{\mathbf{k}0}^R = \frac{1}{2}\left(G_{k+}^R + G_{k-}^R\right), \quad (22a)$$

$$G_{\mathbf{k}x}^R = \frac{n_x}{2n}\left(G_{k+}^R - G_{k-}^R\right), \quad (22b)$$

$$G_{\mathbf{k}y}^R = \frac{n_y}{2n}\left(G_{k+}^R - G_{k-}^R\right), \quad (22c)$$

$$G_{\mathbf{k}z}^R = \frac{n_z}{2n}\left(G_{k+}^R - G_{k-}^R\right). \quad (22d)$$

The Green functions $G_{k\pm}^R = [\varepsilon + \mu - E_\pm + \mathrm{i}\Gamma\mathrm{sgn}(\varepsilon)]^{-1}$ are determined by the chemical potential μ, eigenvalues $E_\pm = n_0 \pm n$ ($n = \sqrt{n_x^2 + n_y^2 + n_z^2}$) and the relaxation rate Γ. The i-th component of the velocity operator is now given by the expression

$$\hat{v}_i = \sum_{j=0,x,y,z}\frac{1}{\hbar}\frac{\partial n_j}{\partial k_i}\sigma_j \equiv \sum_j v_{ij}\sigma_j. \quad (23)$$

We also introduce the general form for the spin operator components:

$$\hat{S}_\alpha = \sum_{j=0,x,y,z} s_{\alpha j}\sigma_j. \quad (24)$$

Combining Eqs. (21)–(24) with Eq. (15) and performing the trace, we obtain the following expressions for the components of current-induced spin polarization:

$$\begin{aligned} S_x(\omega) = \frac{e\hbar}{\omega}E_y\int\frac{d^2\mathbf{k}}{(2\pi)^2}\Big\{&[s_{x0}v_{y0} + s_{xx}v_{yx}]\mathcal{S}_A(\omega) \\ &- s_{xy}v_{yy}\mathcal{S}_B(\omega) \\ &- \left[\frac{n_x}{n}(s_{xx}v_{y0} + s_{x0}v_{yx}) + \frac{n_y}{n}(s_{xy}v_{y0} + s_{x0}v_{yy})\right]\mathcal{S}_C(\omega) \\ &- \mathrm{i}\frac{n_z}{n}[s_{xy}v_{yx} - s_{xx}v_{yy}]\mathcal{S}_D(\omega) \\ &- \frac{1}{n^2}\Big[\left(n_y^2 + n_z^2\right)s_{xx}v_{yx} - n_y^2 s_{xy}v_{yy} \\ &- n_x n_y(s_{xy}v_{yx} + s_{xx}v_{yy})\Big]\mathcal{S}_E(\omega)\Big\}, \end{aligned} \quad (25)$$

$$\begin{aligned} S_y(\omega) = \frac{e\hbar}{\omega}E_y\int\frac{d^2\mathbf{k}}{(2\pi)^2}\Big\{&[s_{y0}v_{y0} + s_{yx}v_{yx}]\mathcal{S}_A(\omega) \\ &- s_{yy}v_{yy}\mathcal{S}_B(\omega) \\ &- \left[\frac{n_x}{n}(s_{yx}v_{y0} + s_{y0}v_{yx}) + \frac{n_y}{n}(s_{yy}v_{y0} + s_{y0}v_{yy})\right]\mathcal{S}_C(\omega) \\ &- \mathrm{i}\frac{n_z}{n}[s_{yy}v_{yx} - s_{yx}v_{yy}]\mathcal{S}_D(\omega) \\ &- \frac{1}{n^2}\Big[\left(n_y^2 + n_z^2\right)s_{yx}v_{yx} - n_y^2 s_{yy}v_{yy} \\ &- n_x n_y(s_{yy}v_{yx} + s_{yx}v_{yy})\Big]\mathcal{S}_E(\omega)\Big\}, \end{aligned} \quad (26)$$

$$\begin{aligned} S_z(\omega) = -\frac{e\hbar}{\omega}E_y\int\frac{d^2\mathbf{k}}{(2\pi)^2}\Big\{&\frac{n_z}{n}s_{zz}v_{y0}\mathcal{S}_C(\omega) \\ &- \mathrm{i}\frac{s_{zz}}{n}[n_x v_{yy} - n_y v_{yx}]\mathcal{S}_D(\omega) \\ &- \frac{n_z}{n^2}s_{zz}[n_x v_{yx} + n_y v_{yy}]\mathcal{S}_E(\omega)\Big\}, \end{aligned} \quad (27)$$

where the functions $\mathcal{S}_A$ to $\mathcal{S}_E$ have the form

$$\begin{aligned} \mathcal{S}_A = &I_{--}^{RA}(\omega) - I_{--}^{RR}(\omega) + I_{++}^{RA}(\omega) - I_{++}^{RR}(\omega) \\ &+ I_{++}^{AA}(-\omega) - I_{--}^{RA}(-\omega) - I_{++}^{RA}(-\omega) + I_{--}^{AA}(-\omega), \end{aligned} \quad (28)$$

$$\begin{aligned} \mathcal{S}_B = &I_{-+}^{RR}(\omega) - I_{-+}^{RA}(\omega) - I_{+-}^{RA}(\omega) + I_{+-}^{RR}(\omega) \\ &+ I_{-+}^{RA}(-\omega) - I_{+-}^{AA}(-\omega) + I_{+-}^{RA}(-\omega) - I_{-+}^{AA}(-\omega), \end{aligned} \quad (29)$$

$$\begin{aligned} \mathcal{S}_C = &I_{--}^{RA}(\omega) - I_{--}^{RR}(\omega) - I_{++}^{RA}(\omega) + I_{++}^{RR}(\omega) \\ &+ I_{--}^{AA}(-\omega) - I_{--}^{RA}(-\omega) + I_{++}^{RA}(-\omega) - I_{++}^{AA}(-\omega), \end{aligned} \quad (30)$$

$$\begin{aligned} \mathcal{S}_D = &I_{-+}^{RA}(\omega) - I_{-+}^{RR}(\omega) - I_{+-}^{RA}(\omega) + I_{+-}^{RR}(\omega) \\ &- I_{+-}^{AA}(-\omega) + I_{-+}^{AA}(-\omega) - I_{-+}^{RA}(-\omega) + I_{+-}^{RA}(-\omega), \end{aligned} \quad (31)$$

$$\begin{aligned}\mathcal{S}_E = {} & I^{RA}_{--}(\omega) - I^{RA}_{-+}(\omega) - I^{RR}_{--}(\omega) + I^{RR}_{-+}(\omega) \\ & - I^{RA}_{+-}(\omega) + I^{RA}_{++}(\omega) + I^{RR}_{+-}(\omega) - I^{RR}_{++}(-\omega) \\ & - I^{AA}_{-+}(-\omega) + I^{AA}_{--}(-\omega) - I^{AA}_{+-}(-\omega) + I^{AA}_{++}(-\omega) \\ & - I^{RA}_{--}(-\omega) + I^{RA}_{-+}(-\omega) + I^{RA}_{+-}(-\omega) - I^{RA}_{++}(-\omega),\end{aligned} \tag{32}$$

and each $I^{XY}_{\alpha\beta}$ denotes integral over ε defined as $I^{XY}_{\alpha\beta}(\omega) = \int \frac{d\varepsilon}{2\pi} f(\varepsilon) G^X_\alpha(\varepsilon+\omega) G^Y_\beta(\varepsilon)$ and $I^{XY}_{\alpha\beta}(-\omega) = \int \frac{d\varepsilon}{2\pi} f(\varepsilon) G^X_\alpha(\varepsilon) G^Y_\beta(\varepsilon-\omega)$. These integrals in their general forms have been derived in Refs. [63] and [64].

III. NONMAGNETIC CASE

In this section, we revisit the model of a nonmagnetic gas with the isotropic k-cubed form of Rashba spin-orbit interaction. In such a case, the Hamiltonian Eq. (1) reduces to the following form:

$$\hat{H} = \frac{\hbar^2 k^2}{2m}\sigma_0 + \mathrm{i}\lambda\left(k_-^3\sigma_+ - k_+^3\sigma_-\right), \tag{33}$$

and the retarded Green's function corresponding to the Hamiltonian Eq. (33) can be presented as

$$G^R_{\mathbf{k}}(\varepsilon) = G^R_{\mathbf{k}0}\sigma_0 + G^R_{\mathbf{k}x}\sigma_x + G^R_{\mathbf{k}y}\sigma_y, \tag{34}$$

with the coefficients

$$G^R_{\mathbf{k}0} = \frac{1}{2}\left(G^R_{k+} + G^R_{k-}\right), \tag{35}$$

$$G^R_{\mathbf{k}x} = \sin(3\phi)\left(G^R_{k+} - G^R_{k-}\right), \tag{36}$$

$$G^R_{\mathbf{k}y} = -\cos(3\phi)\left(G^R_{k+} - G^R_{k-}\right), \tag{37}$$

where ϕ is the angle between the wave vector $\mathbf{k}$ and the axis x, $E_\pm = \frac{\hbar^2 k^2}{2m} \pm \lambda k^3$ denote the energy eigenvalues, and $G^R_{k\pm} = [\varepsilon + \mu - E_\pm + \mathrm{i}\Gamma\,\mathrm{sgn}(\varepsilon)]^{-1}$. The main mechanism responsible for the relaxation is assumed to be the scattering on randomly distributed pointlike impurities. The relaxation rate is obtained as the imaginary part of the self-energy in the Born approximation [62], $\Gamma = \frac{\hbar}{2\tau} = -iIm[\Sigma^R]$ (where τ is the relaxation time). This model has been discussed in the literature also in the context of spin Hall effect [65] and current-induced spin polarization [61] for the 2D hole gas in the zero-temperature limit.

In the nonmagnetic case, only the x component of spin polarization is nonzero and Eq. (25) takes the following form in the dc limit:

$$\begin{aligned}S_x = {} & e\hbar E_y \frac{s_0}{4\pi}\left[3\lambda\int \frac{dkk^4}{2\Gamma}[f'(E_+) - f'(E_-)]\right. \\ & \left. + \frac{\hbar^2}{m}\int \frac{dkk^3}{2\Gamma}[f'(E_+) - f'(E_-)]\right] \\ & - e\hbar E_y \frac{s_1}{4\pi}\left[3\lambda\int \frac{dkk^5}{2\Gamma}\left(\frac{f'(E_+) + f'(E_-)}{1 + (\lambda k^3/\Gamma)^2}\right.\right. \\ & \left.\left. + f'(E_+) + f'(E_-)\right)\right. \\ & \left. + \frac{\hbar^2}{m}\int \frac{dkk^4}{2\Gamma}[f'(E_+) - f'(E_-)]\right].\end{aligned} \tag{38}$$

The integrals over k in the expression above have analytical solutions in the low-temperature limit and lead to the following expression:

$$\begin{aligned}S_x = {} & -\frac{eE_y}{4\Gamma}\hbar s_0\left[3\lambda\left(k^3_{F+}\nu_+ - k^3_{F-}\nu_-\right) + \frac{\hbar^2}{m}\left(k^2_{F+}\nu_+ + k^2_{F-}\nu_-\right)\right] \\ & + \frac{eE_y}{4\Gamma}\hbar s_1\left[3\lambda\left(k^4_{F+}\nu_+ + k^4_{F-}\nu_-\right) + \frac{\hbar^2}{m}\left(k^3_{F+}\nu_+ - k^3_{F-}\nu_-\right)\right. \\ & \left. + 3\lambda\left(\frac{k^4_{F+}\nu_+}{1 + \left(\lambda k^3_{F+}/\Gamma\right)^2} + \frac{k^4_{F-}\nu_-}{1 + \left(\lambda k^3_{F-}/\Gamma\right)^2}\right)\right],\end{aligned} \tag{39}$$

where $k_{F\pm}$ and $\nu_\pm$ are the Fermi wave vectors and densities of states corresponding to the $E_\pm$ energy subbands, respectively. The Fermi wave vectors are connected with the chemical potential μ and electron (hole) density ρ by the following relations: $\mu = E_+(k_{F+}) = E_-(k_{F-})$ and $\rho = (k^2_{F+} + k^2_{F-})/4\pi$. Thus, after some algebraic transformations one finds

$$\begin{aligned}S_x = {} & -\frac{eE_y}{4\Gamma}\hbar s_0\left[2\mu\left(\nu_+ + \nu_-\right) + \lambda\left(k^3_{F+}\nu_+ - k^3_{F-}\nu_-\right)\right] \\ & + \frac{eE_y}{4\Gamma}\hbar s_1\left[2\mu(k_{F+}\nu_+ - k_{F-}\nu_-) + \lambda\left(k^4_{F+}\nu_+ + k^4_{F-}\nu_-\right)\right. \\ & \left. + 3\lambda\left(\frac{k^4_{F+}\nu_+}{1 + (\lambda k^3_{F+}/\Gamma)^2} + \frac{k^4_{F-}\nu_-}{1 + (\lambda k^3_{F-}/\Gamma)^2}\right)\right].\end{aligned} \tag{40}$$

Equation (40) may be treated as a counterpart of the Edelstein result for the linear Rashba model [22]. As the main contribution to the current-induced spin polarization is determined by the diagonal matrix elements of the spin operators (proportional to s_0), the leading term in the equation above is the first one. Thus, similarly as in the case of k-linear Rashba coupling, the external electric field applied to the system induces the nonequilibrium spin polarization, which is aligned in the plane of the 2D gas and perpendicular to the external electric field. In both cases, we also observe linear dependence on the relaxation time $\tau = \frac{\hbar}{2\Gamma}$ and on the Rashba coupling constant. The main difference between the k-linear and k-cubed Rashba models appears in their dependence on the chemical potential. The Edelstein formula does not depend on the chemical potential, whereas the zero-temperature spin polarization for the cubic Rashba model depends almost linearly on μ. This opens the possibility to control the strength of the spin polarization by an external gating or by doping. The dependence of the spin polarization on the chemical potential is a consequence of the fact that the difference between the Fermi wave vectors $k_{F+} - k_{F-}$ depends on the position of the chemical potential in the case of a cubic Rashba coupling. Thus, the shift of the Fermi circles in the presence of an external electric field gives the μ-dependent imbalance between the nonequilibrium spin states in subbands. Note that $k_{F+} - k_{F-}$ is μ-independent for k-linear Rashba interaction and the original Edelstein formula does not depend on the chemical potential.

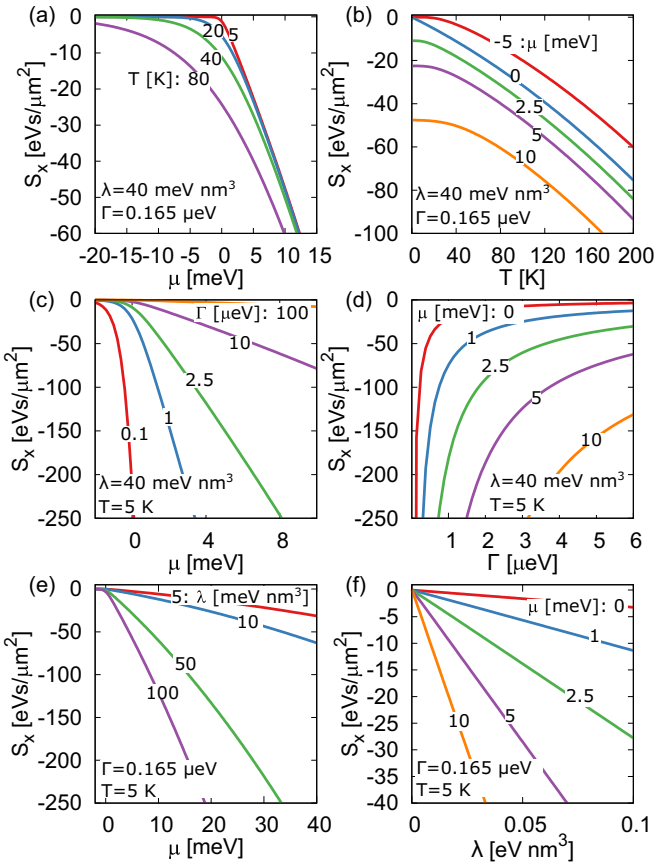

FIG. 2. Current-induced spin polarization in the nonmagnetic case ($h_0 = 0$) as a function of the chemical potential μ (a), (c), (e); temperature T (b), relaxation rate Γ (d), and the spin-orbital coupling parameter λ (f) for fixed parameters as indicated. The external electric field and the effective mass are chosen as $E_y = 1\text{eV/mm}$ and $m = 0.12m_0$, while the Luttinger parameters: $\gamma_1 = 7$ and $\gamma_2 = 0.27\gamma_1$. Other parameters (unless otherwise specified): $\lambda = 0.04\text{eV nm}^3$, $T = 5\text{K}$, and $\Gamma = 1.65 \cdot 10^{-2}\text{meV}$. Cutoff for the integration over $\mathbf{k}$ vector has been assumed as $k_c = k_0/2$, where $k_0 = \hbar^2/3m\lambda$ [65].

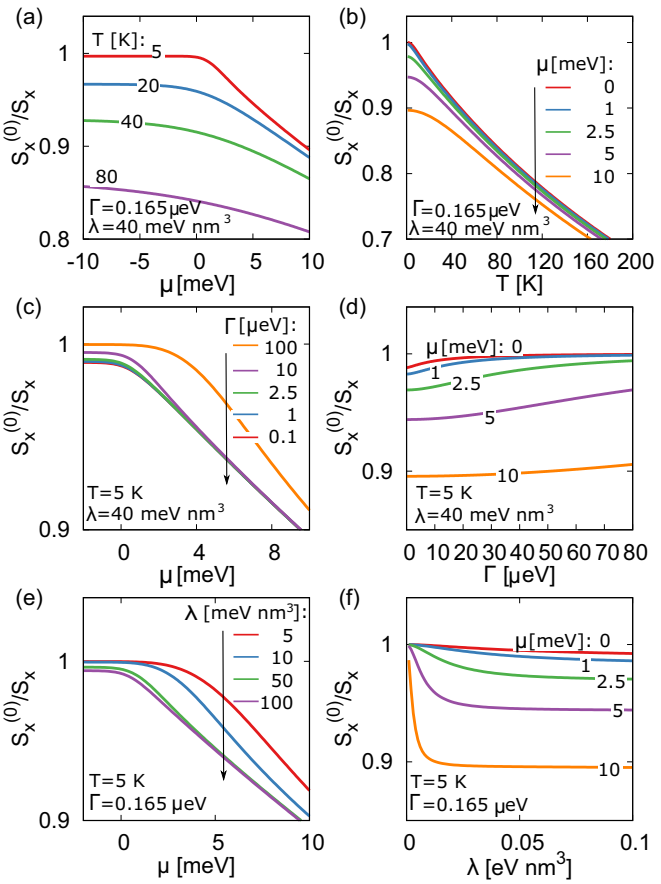

FIG. 3. The ratio of $S_x(s_1 = 0)/S_x(s_1 \neq 0) \equiv S_x^{(0)}/S_x$ in the nonmagnetic case. All parameters are taken as in Fig. 2. This figure shows that the contribution to the spin polarization, related to the parameter s_1 is generally significant and cannot be neglected.

Note that the above results have been obtained in the single loop approximation [62], i.e., the electron scattering is included only in the Green function through the relaxation rate. However, it was reported that for randomly distributed pointlike scatterers, the impurity vertex correction does not provide additional contribution to the transport properties—in other words, the vertex correction to the velocity operator vanishes in this model [66]. Furthermore, the relaxation rate Γ (obtained as an imaginary part of the self-energy in the Born approximation) is the same for both subbands.

Numerical results corresponding to Eq. (38) are presented in Fig. 2. Figures 2(a) and 2(b) show the temperature behavior of the spin polarization. Since the temperature leads to some smearing of the carrier distribution in both subbands, one observes a nonzero spin polarization for negative chemical potentials. Note that in our approach, the chemical potential is fixed while the number of particles can vary. Moreover, spin polarization increases with increasing chemical potential. In a broad range of chemical potentials, this dependence is linear with μ [see Figs. 2(a), 2(c) and 2(e)]. Figures 2(c) and 2(d) highlight the dependence of spin polarization on the relaxation rate Γ. These plots clearly show a fast decrease of the spin polarization with increasing Γ. This decrease, however, depends strongly on the position of the Fermi level, which means that destructive effects associated with scattering on impurities may be slightly tuned by doping/gating of the system. Finally, as the current-induced spin polarization considered here is driven by the spin-orbit interaction, it vanishes for $\lambda = 0$, as shown in Figs. 2(e) and 2(f). The spin polarization also depends linearly on λ as the difference between E_- and E_+ bands changes linearly with λ for a fixed Fermi level.

In our calculations, we have included the terms proportional to s_0 and s_1. The latter was neglected in previous studies [61]. However, from our analysis, it follows that the term proportional to s_1 plays a remarkable role and should be included. In Fig. 3, we show the ratio of spin polarization calculated without (i.e., $S_x(s_1 = 0) = S_x^{(0)}$), and with the terms proportional to s_1 taken into account. Indeed, this figure shows that the term proportional to s_1 can lead to a correction of an order of up to 10% or even larger at higher temperatures and larger Fermi levels, as shown in Figs. 3(a) and 3(b). When the temperature increases, the correction to the spin polarization due to the terms proportional to s_1 decreases with decreasing T for small values of the chemical potential μ, so the corresponding ratio

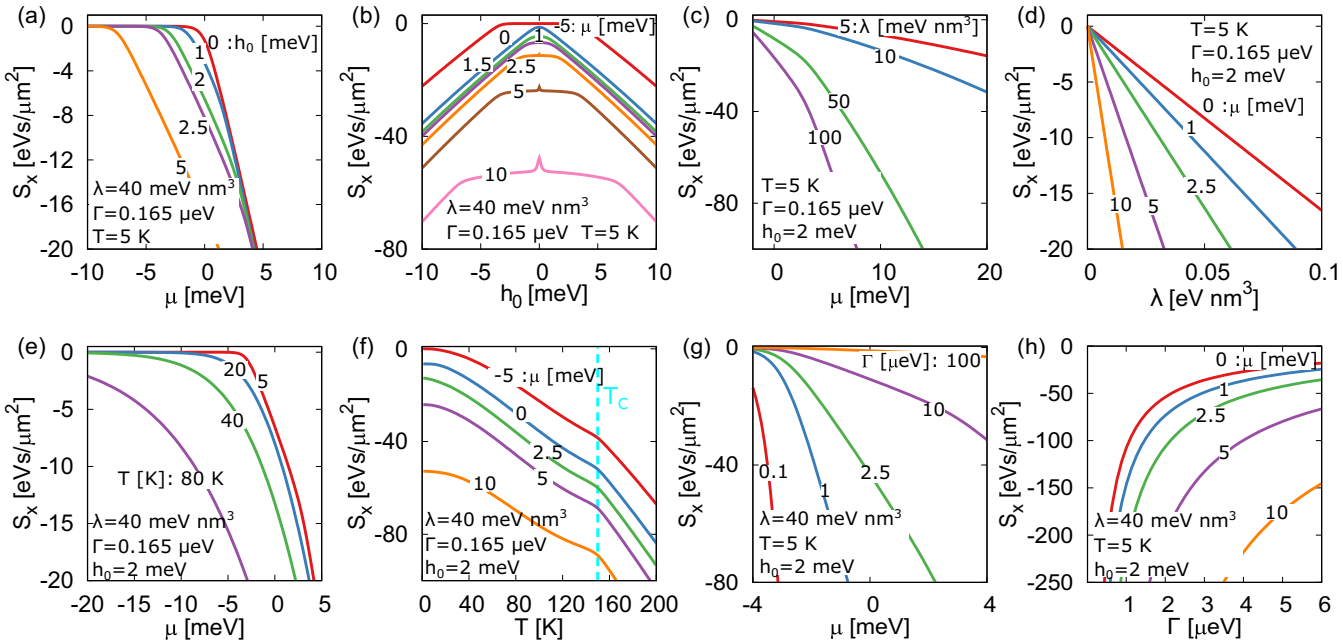

FIG. 4. Current-induced spin polarization in a magnetic case. The x component of the spin polarization for the exchange field normal to the plane of 2DEG (2DHG) is shown as a function of the chemical potential (a,c,e,g), the exchange field h_0 (b), the spin-orbit coupling parameter λ (d), the temperature T (f), and the relaxation rate Γ (h) for fixed parameters, as indicated. Other parameters are the same as in Fig. 2.

$S_x^{(0)}/S_x$ becomes close to 1, see Fig. 3(b). In turn, the ratio $S_x^{(0)}/S_x$ only weakly depends on the impurity scattering rate Γ, as follows from Fig. 3(d). When the Rashba spin-orbit coupling is weak, $S_x^{(0)}$ becomes larger than S_x, i.e., the contribution from the terms proportional to s_1 has opposite sign to that from terms proportional to s_0 and the ratio $S_x^{(0)}/S_x$ exceeds 1, see Fig. 3(f). A similar situation also happens for large values of the chemical potentials, see Fig. 3(e). When the Rashba parameter λ increases, one observes a rapid decrease in $S_x^{(0)}/S_x$ until this ratio saturates at a certain level, see Fig. 3(f).

IV. MAGNETIZED 2D k-CUBED RASHBA GAS

In this section, we consider the general case, when the time-reversal symmetry of the system is broken by the effective exchange field [see Hamiltonian Eq. (1)]. Since the spin-orbit torques play an important role in various spintronics devices, we will analyze a general solution for an arbitrary oriented-exchange field. Such a solution allows one to determine the spin-orbit torque induced by electric field in the system under consideration. Before this, however, we consider two special cases—when the exchange field is oriented perpendicularly to the plane and when the exchange field is oriented in plane of 2D gas.

A. Exchange field perpendicular to the plane of 2D gas

The case of the exchange field being perpendicular to the plane of the 2D gas, i.e., $H_z \neq 0$ and $H_x = H_y = 0$, corresponds either to ferromagnetic LAO/STO layers or to antiferromagnetic system with uncompensated interface. The nonequilibrium spin polarization has then two components, namely the S_x component (which remains also finite for zero exchange field), and the S_y component that is absent in the limit of zero exchange field. The numerical results are presented in Figs. 4 and 5.

The S_x component of spin polarization is only weakly modified by the perpendicular exchange field which introduces, e.g., small nonlinearities in the dependence of S_x on the chemical potential, clearly seen in Figs. 4(a), 4(c), 4(e) and 4(g). These nonlinearities can be attributed to the presence of an energy gap between the subbands. For small values of chemical potential, the component S_x varies monotonically with increasing the magnitude of exchange field, whereas for larger values of μ, this behavior is nonmonotonous, see Fig. 4(b). In the latter case, we observe a local minimum which appears when the Fermi level crosses the bottom edge of the higher subband. For larger values of $|h_0|$, only one subband is occupied and the spin polarization increases with a further increase in the exchange field, see Fig. 4(b). The x component of spin polarization changes linearly with λ, as shown explicitly in Fig. 4(d). The temperature dependence, Fig. 4(f), is similar to that in the absence of exchange field. However, some kinks are well pronounced when the temperature approaches the Curie temperature and the system becomes nonmagnetic.

As the x component of the current-induced spin polarization is only slightly modified by the perpendicular exchange field, the y component of spin polarization appears solely when the exchange field is nonzero. For the perpendicular exchange field, Eq. (26) leads to the following expression for S_y:

$$S_y = eE_y\hbar s_1 \int \frac{d^2\mathbf{k}}{(2\pi)^2}\frac{9H_z k^4\lambda}{4n^3}[f(E_+) - f(E_-)] - eE_y\hbar s_1 \int \frac{d^2\mathbf{k}}{(2\pi)^2}\frac{9H_z k^4\lambda}{4n^2}\frac{\Gamma^2}{n^2+\Gamma^2}[f'(E_+) + f'(E_-)], \quad (41)$$

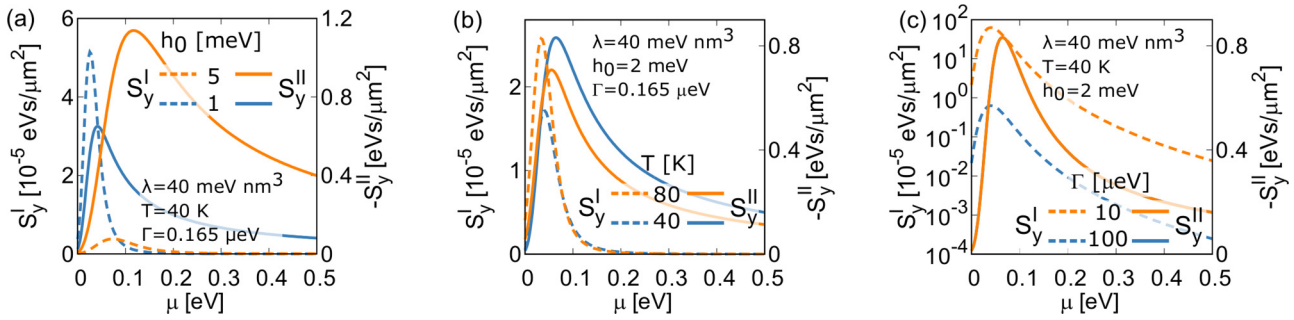

FIG. 5. The contributions S_y^I and S_y^{II} to the y component of current-induced spin polarization for the exchange field normal to the plane of the 2D gas, plotted as a function of the chemical potential μ (for indicated values of the exchange field h_0) (a); temperature T (b); and relaxation rate Γ (c). Other parameters as in Fig. 2.

where n is reduced to the following form: $n = \sqrt{(3H_z)^2 + (2\lambda k^3)^2}/2$.

It should be noted that the current-induced spin polarization, similar to the anomalous or the spin Hall effect, may contain two contributions: A contribution related to the states at the Fermi level, S_α^I, and the second one related to all states below the Fermi level, S_α^{II}:

$$S_\alpha = S_\alpha^I[f'(E_\pm)] + S_\alpha^{II}[f(E_\pm)]. \tag{42}$$

The intrinsic (topological) contribution is easy to identify in Eqs. (25)–(27). In these formulas (when the time-inversion symmetry is broken), the imaginary component of $\mathcal{S}_D$ contributes to the final results and is responsible for the system response from the states below the Fermi level. Thus, the topological contribution appears in our results as a consequence of nonzero exchange coupling and is mostly pronounced in these components which are determined by the exchange field (that is S_y and S_z components). Thus, according to the introduced notation, Eq. (41) may be expressed as $S_y = S_y^I + S_y^{II}$, where

$$S_y^I = -eE_y\hbar s_1 \int \frac{d^2\mathbf{k}}{(2\pi)^2} \frac{9H_z k^4\lambda}{4n^2} \frac{\Gamma^2}{n^2+\Gamma^2}[f'(E_+) + f'(E_-)] \tag{43}$$

and

$$S_y^{II} = eE_y\hbar s_1 \int \frac{d^2\mathbf{k}}{(2\pi)^2} \frac{9H_z k^4\lambda}{4n^3}[f(E_+) - f(E_-)], \tag{44}$$

which is robust against scattering from impurities.

Two important features of the spin polarization follow from the above expression. First, the S_y is linear with respect to the parameter s_1 (which determines the off-diagonal elements of spin operators). This means that even though the contributions associated with s_1 lead only to a small correction to the x component of spin polarization (see the discussion in the preceding section), they are responsible for the appearance of additional components of nonequilibrium spin polarization, e.g., the y component in the case considered in this subsection. Therefore, one cannot ignore the terms related to s_1 if one wants to describe properly the physics of spin polarization in the model under consideration. Second, the S_y component is related to the topological properties of the system and may be expressed in terms of the Berry curvature. For long a relaxation time ($\Gamma \to 0$), the topological component determines the behavior of y component of spin polarization and S_y reduces to S_y^{II}.

As the Berry curvature, $\boldsymbol{\mathcal{B}}_j$, for the j-th subband, is defined by the Berry connection $\boldsymbol{\mathcal{A}}_j(\mathbf{k})$, $\boldsymbol{\mathcal{A}}_j(\mathbf{k}) = \mathrm{i}\langle\Psi_j|\nabla_\mathbf{k}|\Psi_j\rangle$, i.e.,

$$\boldsymbol{\mathcal{B}}_j = \nabla_\mathbf{k} \times \boldsymbol{\mathcal{A}}_j(\mathbf{k}), \tag{45}$$

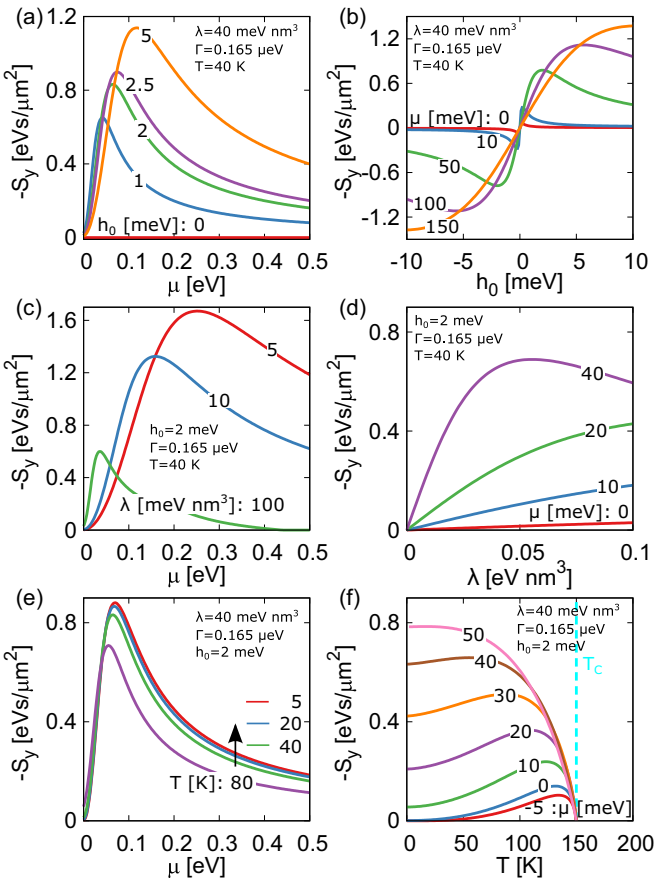

FIG. 6. The y component of the current-induced spin polarization for the exchange field normal to the plane of 2DEG (2DHG) plotted as a function of the chemical potential (a,c,e), exchange field h_0 (b), spin-orbit coupling parameter λ (d), and the temperature T (f) for fixed parameters as indicated. Other parameters as in Fig. 2.

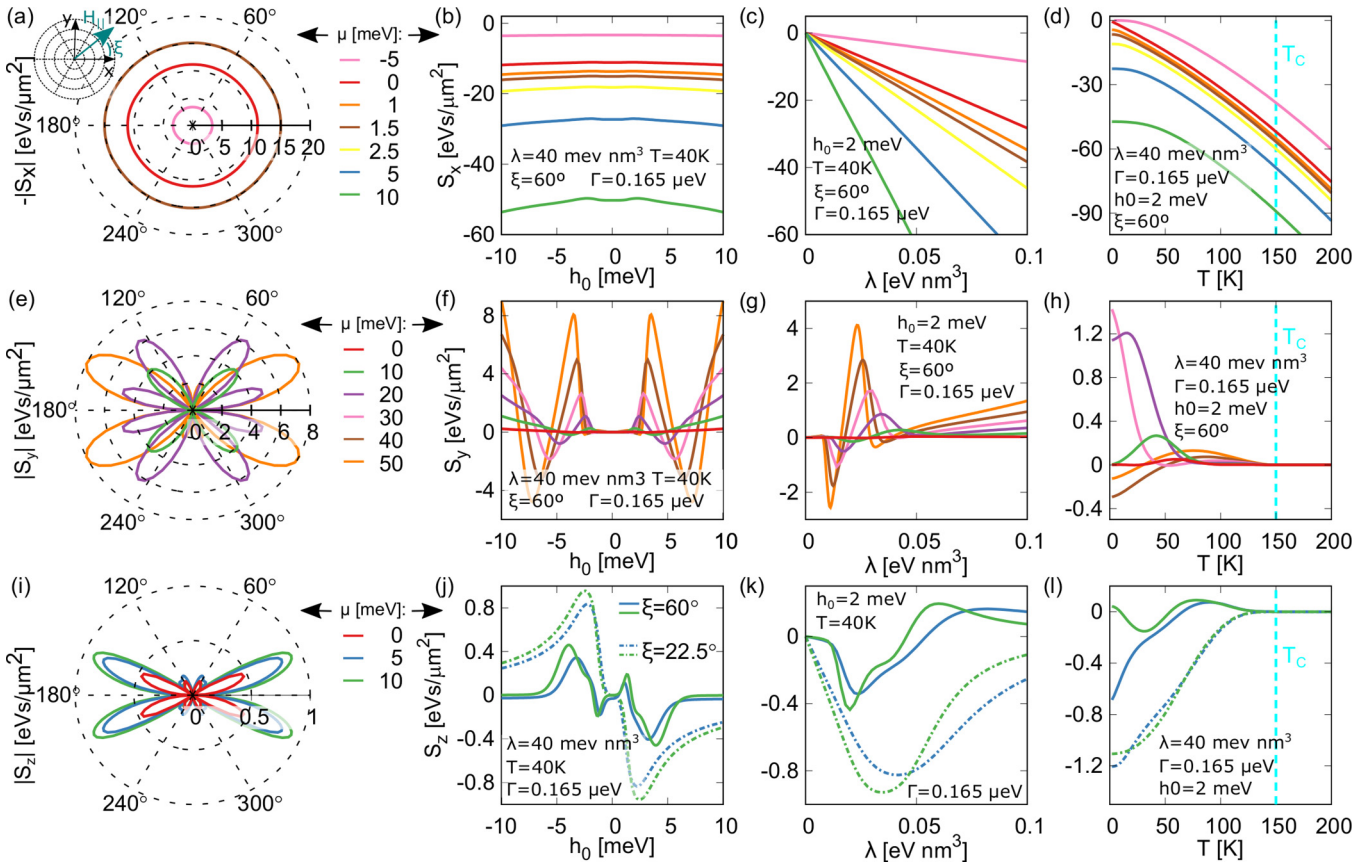

FIG. 7. Current-induced spin polarization in a magnetic case. The spin polarization is shown for the exchange field in the plane of 2DEG (2DHG). The components S_x, (a), S_y, (e), and S_z, (i), as a function of the angle ξ describing the orientation of the in-plane exchange field and for the indicated values of the electrochemical potential μ. The component S_x, S_y, and S_z as a function of the exchange field h_0, (b), (f), (j); Rashba coupling strength λ, (c), (g), (k); and temperature T, (d), (h), (l), respectively. Other parameters as in Fig. 2.

we find for a k-cubed Rashba gas confined in the xy plane, the following explicit form of $\mathcal{B}^z_\pm$:

$$\mathcal{B}^z_\pm = \pm \frac{54 H_z \lambda^2 k^4}{(2n)^3}. \tag{46}$$

Thus, combining Eq. (46) with Eq. (44), we get the following simple expression for the y-component of spin polarization:

$$S_y = S_y^{II} = e\hbar E_y \frac{s_1}{3\lambda} \sum_{j=\pm} \int \frac{d^2\mathbf{k}}{(2\pi)^2} \mathcal{B}^z_j f(E_j). \tag{47}$$

Figure 5 presents the behavior of the individual components of S_y with respect to the change of chemical potential for fixed values of the exchange field, h_0, relaxation rate, Γ, and temperature, T. It is evident that the contribution related to the Berry curvature is five orders of magnitude larger than the contribution related to the states at the Fermi level and therefore determines the y component of the spin polarization. Moreover, as the S_y^{II} component increases with increasing h_0 and decreasing T [Figs. 5(a), 5(b)], the S_y^I component behaves the opposite way—i.e., it decreases with increasing h_0 and increases with increasing temperature. Figure 5(c) shows that S_y^I is highly sensitive to changes in the relaxation rate, Γ, whereas S_y^{II} is robust against the scattering from impurities.

Variation of the total y component of the spin polarization with μ, h_0, λ, and T is presented in Fig. 6. When the Fermi level increases, starting from small values, the S_y component also increases until it reaches its maximal value that depends mainly on the s_1 parameter as well as the strength of the exchange field and the Rashba spin-orbit coupling. Then, the S_y component decreases with a further increase in the Fermi energy, as shown in Figs. 6(a) and 6(b). Furthermore, the maximum in S_y shifts to higher Fermi levels with increasing exchange energy. It is worth noting that the S_y component can change its sign when the magnetization is reversed. For relatively small Rashba spin-orbit coupling strength and small values of μ, the S_y component increases monotonously with λ, as shown in Figs. 5(c) and 5(d). However, for larger values of μ, the S_y component initially increases with λ and then, upon reaching a maximum, it decreases with a further increase in λ. This behavior is different from that found for the S_x component. Since the S_y component is strongly dependent on the exchange field, it is also highly sensitive to changes in temperatures, as shown in Figs. 6(e) and 6(f). For small Fermi levels, the maximal value of S_y occurs when T approaches Curie temperature $T_C = 150$ K and then it quickly disappears when the exchange field vanishes, i.e., when $H_z(T = T_C) = 0$. For higher Fermi levels, the maximal value occurs at low temperatures.

B. Exchange field in the plane of 2D gas

We consider now the case when the exchange field is in the plane of the 2DEG, i.e., when $H_z = 0$ and $H_x, H_y \neq 0$. Similarly, as in the case described above, the x component of spin polarization is only weakly modified by the in-plane exchange field—see Figs. 7(a)–7(d). On the other hand, when the exchange field is in the plane of 2D gas, both y and z components of the spin polarization can occur and significantly depend on the orientation and strength of the exchange field. For example, the S_y component [see Fig. 7(e)] is absent when the in-plane field is parallel to either x or y axis (i.e., when $\xi = 0^\circ$ or $\xi = 90^\circ$), whereas the S_z component vanishes for the in-plane field oriented along the x axis and takes its maximal value for exchange field oriented along the y axis, see Fig. 7(i). The x and y components are both nonzero when the in-plane exchange field is aligned between the x and y axes. The specific positions of the maxima in S_y depend on the Fermi level. Both S_y and S_z components, however, are one to two orders of magnitude smaller than the S_x component.

The behavior of the spin polarization presented in Fig. 7 indicates a strong interplay between the effective field induced by the spin-orbit coupling and the in-plane exchange field. The dependence of the S_y component on the exchange field and the Rashba coupling parameter is presented in Figs. 7(f) and 7(g), for $\xi = 60^\circ$. This component behaves symmetrically with respect to the magnetization reversal, and its sign can be changed by tuning the magnitude of the exchange field or the spin-orbit coupling strength. The temperature-dependence of S_y, shown in Fig. 7(h), indicates that relatively low temperatures are necessary to have remarkable values of S_y and that the S_y component vanishes when T approaches the Curie temperature.

The S_z component, in turn, is antisymmetric with respect to the sign reversal of the in-plane exchange field. A nonzero value of S_z means that the vector of spin polarization is tilted out of the plane of 2D gas. In Figs. 7(j)–7(k), the dependence of z component of the spin polarization on the magnitude of the exchange field and the Rashba coupling parameter is presented for two orientations of the field, i.e., for $\xi = 22.5^\circ$ (when the z component assumes its maximal values) and $\xi = 60^\circ$. The S_z component is larger for higher values of the chemical potential. For $\xi = 22.5^\circ$, the $|S_z|$ component displays only one peak in the dependence on $|h_0|$, see Fig. 7(j). For $\xi = 60^\circ$, the $|S_z|$ curve displays two peaks. This might be attributed to the anisotropy introduced by the in-plane field and greater separation in the **k**-vector space of the E_- and E_+ states for $\xi = 60^\circ$ than for $\xi = 22.5^\circ$. Similar behavior is visible in Fig. 7(k), where the S_z component is shown as a function of the Rashba spin-orbit coupling strength λ. Similarly, as in the case of the S_y component, the S_z component is substantial for low temperatures and disappears when the temperature approaches the Curie temperature, where the exchange field vanishes.

V. SUMMARY

We presented a detailed study of the current-induced spin polarization in a 2D electron gas with an isotropic k-cubed Rashba spin-orbital coupling. The model under consideration is useful for understanding the nonequilibrium spin polarization and the spin dynamics in some p-doped semiconductor quantum wells, as well as in electron gases at the interfaces of oxides perovskites.

We have shown that the contribution related to the parameter s_1 should not be omitted. This contribution in a nonmagnetic case modifies the spin polarization by about 10%; however, in the magnetic case, it is responsible for the components that are absent in the limit of a zero exchange field. We also discussed briefly the relation of some terms in the spin polarization with the Berry curvature. Generally, one can expect that the induced spin polarization in a magnetic system leads to a torque on the local magnetization, which in turn can modify the spin dynamics.

ACKNOWLEDGMENTS

This work was partially supported by The Polish Ministry of Science and Higher Education, project Iuventus Plus No. 0083/IP3/2015/73 and by the German Research Foundation (DFG) under SFB 762. A.D. acknowledges the support from the Foundation for Polish Science (FNP).

[1] A. Soumyanarayanan, N. Reyren, A. Fert, and Ch. Panagopoulos, Nature **539**, 509 (2016).
[2] F. Hellman, A. Hoffmann, Y. Tserkovnyak, G. S. D. Beach, E. E. Fullerton, Ch. Leighton, A. H. MacDonald, D. C. Ralph, D. A. Arena, H. A. Dürr *et al.*, Rev. Mod. Phys. **89**, 025006 (2017).
[3] J. Schliemann, Rev. Mod. Phys. **89**, 011001 (2017).
[4] P. Gambardella and I. M. Miron, Philos. Trans. R. Soc. A **369**, 3175 (2011).
[5] K. S. Novoselov, A. Mishchenko, A. Carvalho, and A. H. Castro Neto, Science **353**, 9439 (2016).
[6] A. K. Geim and I. V. Grigorieva, Nature **499**, 419 (2013).
[7] P. Zubko, S. Gariglio, M. Gabay, P. Ghosez, and J.-M. Triscone, Annu. Rev. Condens. Matter Phys. **2**, 141 (2011).
[8] J. Fabian, A. Matos-Abiague, C. Ertler, P. Stano, and I. Zutic, Acta Physica Slovaca **57**, 565 (2007).
[9] J. E. Hirsch, Phys. Rev. Lett. **83**, 1834 (1999).
[10] M. I. Dyakonov and V. I. Perel, Pis'ma Zh. Eksp. Teor. Fiz. **13**, 657 (1971) [JETP Lett. **13**, 467 (1971)].
[11] M. I. Dyakonov and A. V. Khaetskii, in *Spin Physics in Semiconductors*, edited by M. I. Dyakonov (Springer-Verlag, Berlin, Heidelberg, 2008), Chap. 8.
[12] B. Özyilmaz, A. D. Kent, J. Z. Sun, M. J. Rooks, and R. H. Koch, Phys. Rev. Lett. **93**, 176604 (2004).
[13] S. I. Kiselev, J. C. Sankey, I. N. Krivorotov, N. C. Emley, R. J. Schoelkopf, R. A. Buhrman, and D. C. Ralph, Nature **425**, 380 (2003).
[14] T. Jungwirth, J. Wunderlich, and K. Olejnik, Nat. Mater. **11**, 382 (2012).
[15] J. Sinova, S. O. Valenzuela, J. Wunderlich, C. H. Back, and T. Jungwirth, Rev. Mod. Phys. **87**, 1213 (2015).

[16] L. Liu, T. Moriyama, D. C. Ralph, and R. A. Buhrman, Phys. Rev. Lett. **106**, 036601 (2011).

[17] I. M. Miron, K. Garello, G. Gaudin, P.-J. Zermatten, M. V. Costache, S. Auffret, S. Bandiera, B. Rodmacq, and A. S. P. Gambardella, Nature **476**, 189 (2011).

[18] L. Liu, Ch.-F. Pai, Y. Li, H. W. Tseng, D. C. Ralph, and R. A. Buhrman, Science **336**, 555 (2012).

[19] M. Cecot, Ł. Karwacki, W. Skowronski, J. Kanak, J. Wrona, A. Żywczak, L. Yao, S. Dijken, J. Barnaś, and T. Stobiecki, Sci. Rep. **7**, 968 (2017).

[20] M. I. Dyakonov and V. I. Perel, Phys. Lett. A **35**, 459 (1971).

[21] E. L. Ivchenko and G. E. Pikus, Pis'ma Zh. Eksp. Teor. Fiz. **27**, 640 (1978) [JETP Lett. **27**, 604 (1978)].

[22] V. M. Edelstein, Solid State Commun. **73**, 233 (1990).

[23] A. G. Aronov and Yu. B. Lyanda-Geller, Pis'ma Zh. Eksp. Teor. Fiz. **50**, 398 (1989) [JETP Lett. **50**, 431 (1989)].

[24] C. Gorini, A. Maleki Sheikhabadi, Ka Shen, I. V. Tokatly, G. Vignale, and R. Raimondi, Phys. Rev. B **95**, 205424 (2017).

[25] A. Maleki Sheikhabadi and R. Raimondi, Condens. Matter **2**, 17 (2017).

[26] K. Shen, G. Vignale, and R. Raimondi, Phys. Rev. Lett. **112**, 096601 (2014).

[27] A. Ohtomo, D. Muller, J. Grazul, and H. Hwang, Nature (London) **419**, 378 (2002).

[28] A. Ohtomo and H. Hwang, Nature (London) **427**, 423 (2004).

[29] A. Brinkma, M. Huijben, M. van Zalk, J. Huijben, U. Zeitler, J. C. Maan, W. G. van der Wiel, G. Rijnders, D. H. A. Blank, and H. Hilgenkamp, Nat. Matter. **6**, 493 (2007).

[30] A. Joshua, S. Pecker, J. Ruhman, E. Altman, and S. Ilani, Nature Commun. **3**, 1129 (2012).

[31] S. Thiel, G. Hammerl, A. Schmehl, C. W. Schneider, and J. Mannhart, Science **313**, 1942 (2006).

[32] A. D. Caviglia, Gariglio, N. Reyren, D. Jaccard, T. Schneider, M. Gabay, S. Thiel, G. Hammerl, J. Mannhart, and J.-M. Triscone, Nature **456**, 624 (2008).

[33] A. D. Caviglia, M. Gabay, S. Gariglio, N. Reyren, C. Cancellieri, and J.-M. Triscone, Phys. Rev. Lett. **104**, 126803 (2010).

[34] C. A. Jackson and S. Stemmer, Phys. Rev. B **88**, 180403 (2013).

[35] T. Kimura, T. Goto, H. Shintani, K. Ishizaka, T. Arima, and Y. Tokura, Nature **426**, 55 (2003).

[36] Y. Tokura and S. Seki, Adv. Mater. **22**, 1554 (2009).

[37] A. Glavic, C. Becher, J. Voigt, E. Schierle, E. Weschke, M. Fiebig, and T. Bruckel, Phys. Rev. B **88**, 054401 (2013).

[38] J. Ruhman, A. Joshua, S. Ilani and E. Altman, Phys. Rev. B **90**, 125123 (2014).

[39] D. Stornaiuolo, S. Gariglio, A. Fete, M. Gabay, D. Li, D. Massarotti, and J.-M. Triscone, Phys. Rev. B **90**, 235426 (2014).

[40] J. Biscaras, N. Bergeal, S. Hurand, C. Feuillet-Palma, A. Rastogi, R. C. Budhani, M. Grilli, S. Caprara, and J. Lesueur, Nat. Mater. **12**, 542 (2013).

[41] D. Bucheli, M. Grilli, F. Peronaci, G. Seibold, and S. Caprara, Phys. Rev. B **89**, 195448 (2014).

[42] E. Lesne, Yu Fu, S. Oyarzun, J. C. Rojas-Sanchez, D. C. Vaz, H. Naganuma, G. Sicoli, J.-P. Attane, M. Jamet, E. Jacquet, J.-M. George, A. Barthelemy, H. Jaffres, A. Fert, M. Bibes, and L. Vila, Nat. Mater. **15**, 1261 (2016).

[43] M. Wahler, N. Homonnay, T. Richter, A. Müller, Ch. Eisenschmidt, B. Fuhrmann, and G. Schmidt, Sci. Rep. **6**, 28727 (2016).

[44] G. Seibold, S. Caprara, M. Grilli, and R. Raimondi, Phys. Rev. Lett. **119**, 256801 (2017).

[45] C. Cen, S. Thiel, G. Hammerl, C. W. Schneider, K. E. Andersen, C. S. Hellberg, J. Mannhart, and J. Levy, Nat. Mater. **7**, 298 (2008).

[46] L. Li, C. Richter, J. Mannhart, and R. C. Ashoori, Nat. Phys. **7**, 762 (2011).

[47] A. J. Bert, B. Kalisky, Ch. Bell, M. Kim, Y. Hikita, H. Y. Hwang, and K. A. Moler, Nat. Phys. **7**, 767 (2011).

[48] R. Bistritzer, G. Khalsa, and A. H. MacDonald, Phys. Rev. B **83**, 115114 (2011).

[49] G. Khalsa and A. H. MacDonald, Phys. Rev. B **86**, 125121 (2012).

[50] G. Khalsa, B. Lee, and A. H. MacDonald, Phys. Rev. B **88**, 041302(R) (2013).

[51] J. Zhou, W.-Y. Shan, and Di Xiao, Phys. Rev. B **91**, 241302(R) (2015).

[52] R. Winkler, *Spin-Orbit Coupling Effects in Two-Dimensional Electron and Hole Systems* (Springer-Verlag, Berlin/Heidelberg, 2003).

[53] L. W. van Heeringen, G. A. de Wijs, A. McCollam, J. C. Maan, and A. Fasolino, Phys. Rev. B **88**, 205140 (2013).

[54] L. W. van Heeringen, A. McCollam, G. A. de Wijs, and A. Fasolino, Phys. Rev. B **95**, 155134 (2017).

[55] H. Nakamura, T. Koga, and T. Kimura, Phys. Rev. Lett. **108**, 206601 (2012).

[56] H. Liang, L. Cheng, L. Wei, Z. Luo, G. Yu, Ch. Zeng, and Z. Zhang, Phys. Rev. B **92**, 075309 (2015).

[57] A. D. Caviglia, S. Gariglio, C. Cancellieri, B. Sacépé, A. Fête, N. Reyren, M. Gabay, A. F. Morpurgo, and J.-M. Triscone, Phys. Rev. Lett. **105**, 236802 (2010).

[58] A. H. A. Hassan, R. J. H. Morris, O. A. Mironov, S. Gabani, A. Dobbie, and D. R. Leadley, Appl. Phys. Lett. **110**, 042405 (2017).

[59] R. Moriya, K. Sawano, Y. Hoshi, S. Masubuchi, Y. Shiraki, A. Wild, C. Neumann, G. Abstreiter, D. Bougeard, T. Koga, and T. Machida, Phys. Rev. Lett. **113**, 086601 (2014).

[60] Z. Zhong, A. Toth, and K. Held, Phys. Rev. B **87**, 161102(R) (2013).

[61] C.-X. Liu, B. Zhou, S.-Q. Shen, and B.-F. Zhu, Phys. Rev. B **77**, 125345 (2008).

[62] G. D. Mahan, *Many Particle Physics* (Kluwer Academic/Plenum Publishers, New York, 2000).

[63] A. Dyrdal, J. Barnaś, and V. K. Dugaev, Phys. Rev. B **95**, 245302 (2017).

[64] A. Dyrdal, J. Barnaś, and V. K. Dugaev, Phys. Rev. B **94**, 035306 (2016).

[65] J. Schliemann and D. Loss, Phys. Rev. B **71**, 085308 (2005).

[66] S. Murakami, Phys. Rev. B **69**, 241202(R) (2004).